Angular distribution measurements of neutron elastic scattering on natural carbon

G. Gkatis,[1,2] E. Pirovano,[3] M. Diakaki,[2] G. Noguere,[1] M. Nyman,[4] A. Oprea,[5] C. Paradela,[5] and A. J. M. Plompen[5,*]

[1]*CEA/DES/IRESNE/DER/SPRC/LEPh, Cadarache, F-13108 Saint Paul Lez Durance, France*
[2]*Department of Physics, National Technical University of Athens, GR-15780 Athens, Greece*
[3]*Physikalisch-Technische Bundesanstalt, D-38116 Braunschweig, Germany*
[4]*Department of Chemistry, University of Helsinki, FI-00014 Helsinki, Finland*
[5]*Joint Research Centre, European Commission, B-2440 Geel, Belgium*

(Received 11 March 2024; accepted 22 July 2024; published 11 September 2024)

The angular distributions of neutron elastic scattering on natural carbon were studied in the fast neutron energy region between 1 and 8 MeV. The experiments were carried out at the white neutron source of the Geel Electron Linear Accelerator (GELINA) facility by using thin and thick natural carbon samples. This work demonstrates the need for using thin samples to avoid strong multiple scattering effects. Neutrons and γ rays from scattering were detected using the ELastic and Inelastic Scattering Array (ELISA), a setup consisting of 32 liquid organic scintillators. The n-γ separation was achieved via pulse-shape analysis. For each sample a different approach in methodology is studied, one based on a global response function model and another one based on a per-detector model. The detectors are placed at eight different detection angles between 16° and 164° with respect to the neutron beam direction, allowing the simultaneous calculation of both the differential and the integral cross section by implementing the Gauss-Legendre quadrature rule. The neutron flux was measured with a ^{235}U ionization chamber. The angular distributions were extracted relative to the ^{235}U(n, f) cross section. The results are compared with other experimental data available in the EXFOR library, along with the most recent nuclear data evaluations. The angle-integrated cross sections are in excellent agreement with the nuclear data evaluations and for the angular distributions, ENDF/B-VIII.0 is better reproducing the experimental data in all eight detection angles.

DOI: 10.1103/PhysRevC.110.034609

I. INTRODUCTION

Carbon is an important material, present in a broad spectrum of nuclear technology applications. In nuclear reactors, graphite is used as moderator and reflector due to its excellent neutron scattering properties and high thermal conductivity. Additionally, carbon fiber-reinforced materials are considered an attractive choice for use in structural components of next-generation reactors [1–3]. Therefore, accurate neutron data are essential for the design, safe operation, and development of advanced reactor systems, especially in the energy region from hundreds of keV to few MeV.

In many laboratories, measurements of the cross section of neutron elastic scattering by carbon are used to calibrate detectors, monitor their stability, and validate experimental results. It is well matched for such applications because the cross section is reliably known with an uncertainty below 1% up to 4.8 MeV incident neutron energy. Furthermore, the differential cross section is proposed as a standard by the IAEA, for neutron energies below 1.8 MeV [4].

When it comes to the nuclear data evaluations of carbon, two different approaches have been adopted in the recent years. In the JEFF-3.3 evaluated library [5], released in 2017, only one file that corresponds to the elemental cross section is available, based on the ENDF/B-VI.1 evaluation by Fu [6,7] for incident neutron energies below 20 MeV. In the ENDF/B-VIII.0 library [8], released in 2018, separate files for the isotopic description of the cross section for both ^{12}C (98.94%) and ^{13}C (1.06%) are provided. This is the first ENDF/B version providing isotopic instead of elemental cross sections for the case of carbon and it was achieved by performing a detailed R-matrix analysis for the description of the ^{13}C system using the EDA code [9], resulting in a new evaluation for the neutron cross sections of ^{12}C at energies below 6.5 MeV [10]. Additionally, changes were made in the Legendre coefficients that represent the angular distributions of neutron elastic and inelastic scattering. More recently, the JENDL-5 evaluated library [11], released in 2021, also provided an evaluation of both isotopes. The same methodology was followed, performing an R-matrix analysis for the ^{13}C compound system using the AMUR code [12] and fitting the experimental total cross sections up to 4.4 MeV (inelastic scattering threshold). At the same time, the Legendre coefficients for the elastic scattering were carefully monitored in order to reproduce experimental

*Contact author: arjan.plompen@ec.europa.eu

TABLE I. Neutron elastic scattering cross section data available in the EXFOR library [13], in chronological order. The name of the first author, the year of publication, the neutron energy range under study, the quantity (CS and/or DA) and the number of points are listed.

Reference		En range (MeV)	Quantity (Points)	
Macphail (1940)	[14]	2.34-2.80	CS(6)	
Little Jr. (1955)	[15]	2.70		DA(9)
Jennings (1955)	[16]	4.40		DA(1)
Walt (1955)	[17]	4.10	CS(1)	DA(8)
Willard (1955)	[18]	0.55-1.50	CS(3)	DA(25)
Muehlhause (1956)	[19]	1.66		DA(35)
Beyster (1956)	[20]	7.00		DA(105)
Langsdorf Jr. (1957)	[21]	0.03-1.78	CS(34)	DA(370)
Wills Jr. (1958)	[22]	1.45-4.10		DA(107)
Hosoe (1959)	[23]	2.85-3.00		DA(56)
Haddad (1959)	[24]	6.00-7.00	CS(3)	DA(30)
Bostrom (1959)	[25]	4.21-7.58	CS(3)	DA(38)
Lane (1961)	[26]	1.96-2.24		DA(256)
Lane (1969)	[27]	0.50-2.00	CS(39)	DA(243)
Perey (1969)	[28]	4.60-8.56	CS(13)	DA(265)
Ahmed (1970)	[29]	0.50-2.00		DA(427)
Mcdaniel (1972)	[30]	7.48		DA(13)
Galati (1972)	[31]	3.03-6.94		DA(476)
Knox (1973)	[32]	2.63	CS(1)	DA(8)
Velkley (1973)	[33]	7.20-9.00		DA(106)
Hollandsworth (1975)	[34]	7.55		DA(6)
Perey (1978)	[35]	5.22-8.69	CS(40)	DA(670)
Smith (1979)	[36]	1.50-3.99	CS(31)	DA(438)
Pirovano (2019)	[37]	1.99-7.99	CS(140)	DA(1120)
Ramirez (2022)	[38]	0.50-7.96	CS(66)	DA(739)

data of the differential cross section with respect to angle. Even though in all these evaluations special care was given to reproduce the standard cross section until 1.8 MeV, discrepancies in the neutron angular distributions up to 22% are observed above this energy.

In Table I the experimental data available in the EXFOR [13] library for the cross sections of neutron elastic scattering on natural carbon in the incident neutron energy range between 1 and 8 MeV are presented. An in-depth examination of the existing data reveals numerous issues. For the elastic scattering cross section (CS), it is observed that only a few data sets are available, each one covering different parts of the energy range with limited to zero overlap between the different experiments. Especially in the energy range from 4 to 6 MeV, only a handful of cross section values are reported, with uncertainties reaching 20%, not accurate enough to sufficiently describe the cross section in this region. In the case of the angular distributions (DA), even though more experimental data are available, the energy and angle coverage is limited due to the fact that all the reported measurements have been performed with quasi-monoenergetic neutron beams, and a few detectors placed in specific detection angles. Additionally, discrepancies of the order of 25% between the different data sets are observed.

The objective of this work is to provide, for the first time, high-resolution cross section data of neutron elastic scattering on natural carbon in the fast neutron energy region (1 to 8 MeV). These new data will play a crucial role in clearing out discrepancies between experimental data, and assist in the further development of the current evaluated libraries of carbon. Two measurements were performed, using two high purity natural carbon samples, a thick (Ref. [39]) and a thin one, a white neutron source, and a detection setup consisting of 32 liquid organic scintillators for the detection of the scattered neutrons, which will be described in the next section.

TABLE II. Dimensions and areal densities of the two natural carbon samples used at the two experiments.

Sample	Thick	Thin
Mass (g)	130.42(1)	27.70(1)
Diameter (mm)	100.0(1)	100.0(1)
Thickness (mm)	9.9(1)	2.0(1)
Areal mass density (g/cm^2)	1.661(3)	0.352(1)
Areal atom density (atoms/barn)	0.0832(2)	0.0176(1)

II. EXPERIMENTAL CONDITIONS

A. Neutron source

The measurements were performed at the GELINA neutron time-of-flight facility of the European Commission's Joint Research Centre in Geel (EC-JRC Geel) [40,41]. GELINA employs a linear electron accelerator to produce pulsed white neutron beams. In practice, electrons are accelerated and then directed to a depleted uranium disk (neutron producing target) in pulses of 2 ns duration. The interaction between the high-energy electrons and the target material produces photons via the bremsstrahlung process and then neutrons via photonuclear reactions in the uranium nuclei [^{238}U(γ, n)-^{238}U(γ, f)]. The produced neutrons cover a broad energy spectrum up to 20 MeV. They are emitted isotropically, and then are collimated to form beams directed to the different measuring stations.

B. Carbon samples

For the experiments, two high purity carbon samples were used. Table II presents the characteristics of the samples. The estimated areal densities of the thick and the thin targets were 1.661(3) g/cm^2 and 0.352(1) g/cm^2, respectively. The reason behind choosing targets of different thickness was to study the multiple scattering effect. The graphite samples were placed at a 27.037(5) m distance from the neutron producing target, at the sample position of the spectrometer, 29.5(1) cm away from the detectors. The neutron beam diameter at the sample position was measured using a photographic film and was found to be 4.9(2) cm.

C. ELISA spectrometer

For the detection of the scattered neutrons the ELISA (ELastic and Inelastic Scattering Array) spectrometer was employed (Fig. 1). The setup is described in detail in

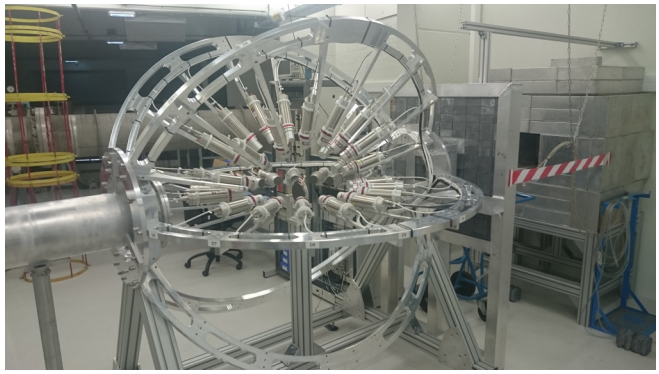

FIG. 1. The ELISA setup, placed at the 30 m station of flight path 1. The neutron beam comes from the right, passes through the fission chamber located behind the lead wall, and reaches the scattering sample.

Refs. [37,39,42–44], here only a short report of the main parts is given. The spectrometer consists of 32 liquid organic scintillator detectors. For half of the detectors the neutron detection is based on the *n*-*p* scattering (EJ301 scintillator material) while the other half is utilizing the *n*-*d* scattering (EJ315 scintillator material). These scintillators possess high speed and exhibit a time resolution of less than 1 ns, making them ideal for time-of-flight measurements. Also, they are well suited for neutron spectrometry because distinguishing between photons and neutrons can be accomplished through pulse shape analysis.

In the setup, the detectors are positioned in four sets of eight scintillators each, mounted at specific angles with respect to the neutron beam direction (Fig. 2). The detection angles were chosen so that their respective cosines reproduce the zeros of the Legendre polynomials of the eighth order. This allows the calculation of the angle integrated cross section $\sigma_{\mathrm{el}}(E)$ using the Gauss-Legendre quadrature method:

$$\sigma_{\mathrm{el}}(E) = 2\pi \sum_{i=1}^{8} w_i \frac{d\sigma_{\mathrm{el}}}{d\Omega}(E, \theta_i), \tag{1}$$

where $\frac{d\sigma_{\mathrm{el}}}{d\Omega}(E, \theta_i)$ is the differential elastic neutron scattering cross section as a function of the detection angle θ_i, and w_i are the corresponding weighting factors.

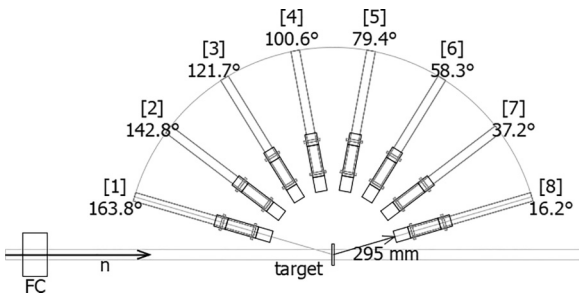

FIG. 2. Schematic of one of the four sets with the eight detectors mounted at specific detection angles. A full description of the measurement geometry is given in Ref. [39].

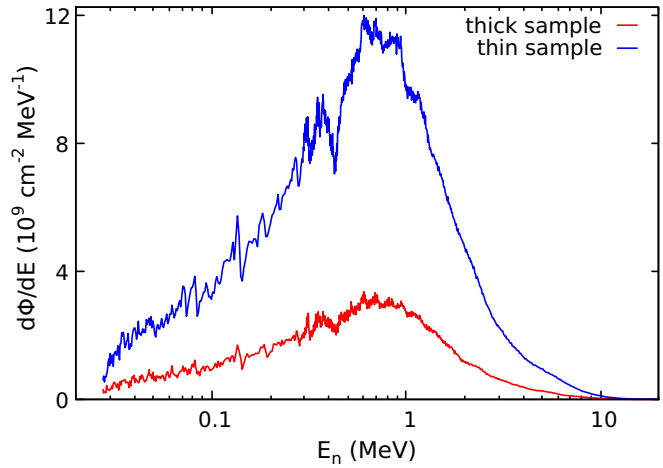

FIG. 3. Neutron fluence impinged on the natural carbon samples with respect to the incident neutron energy. The curves correspond to the total duration of the sample-in measurements that amounts to 120 hours for the thick (red line) and 360 hours for the thin (blue line) samples.

For the measurement of the incident neutron flux a ^{235}U ionization chamber is placed at 1.37 m upstream the sample position. Inside the chamber 8 UF_4 deposits on five aluminum foils are included. The deposits have a diameter of 70 mm and the total areal density of ^{235}U in the chamber is 4095 (4) μg/cm^2, which was experimentally determined via α counting. As described in Ref. [39] the incident neutron fluence is calculated relative to the standard $^{235}\mathrm{U}(n, f)$ reaction cross section by correlating the fission fragment counts recorded in the chamber with the number of incident neutrons. In Fig. 3 the neutron fluence impinged on the carbon samples during the measurements is presented.

The data acquisition system for the detectors is based on digitizers. The signals from the scintillators are read out by ADQ14DC-4A-VG-PXIe digitizers running at 500 MS/s sampling frequency and with 14-bit amplitude resolution. For the data acquisition system of the ionization chamber conventional NIM electronics were utilized. All acquired data are saved in list-mode files for offline analysis.

For each sample two different kind of measurements were carried out. One where the sample was placed in the beam path (sample-in) lasted 120 hours for the thick and 360 hours for the thin sample, and the other without the sample (sample-out) lasted 120 hours for the thick and 240 hours for the thin sample. The sample-out measurements were performed in order to determine the contribution of in-beam neutrons scattered in the air and surrounding materials and then reaching one of the detectors. In both experiments, the sample-in and sample-out irradiation times are almost equally long to ensure that background subtraction will not dominate the uncertainty. The big difference in the measurement time of the two samples (the measurement of the thick sample was one-third that of the thin one) was due to the thick sample's fivefold greater mass resulting in satisfactory statistics faster.

III. ANALYSIS

The neutron differential elastic scattering cross section was calculated via the expression

$$\frac{d\sigma_{\rm el}}{d\Omega}(E,\theta) = \frac{N'_{\rm el}(E,\theta)}{\Delta\Omega\rho_T\Phi(E)A_b}, \quad (2)$$

where E is the incident neutron energy, $N'_{\rm el}$ is the corrected counts of elastic scattering events, $\Delta\Omega$ is the detector's solid angle, ρ_T is the areal density of the carbon sample in atoms/barn (Table II), $\Phi(E)$ is the neutron fluence (Fig. 3), and A_b is the cross-sectional area of the neutron beam, which is also included in the calculation of the neutron fluence and therefore is canceled out. Throughout the text, angle θ will implicitly represent the eight angles of the ELISA setup.

The elastic scattering reaction yield was determined by analyzing the scintillator data. The method to analyze data obtained with the ELISA spectrometer is described in detail in Refs. [37,39], here only a brief overview of the most important components of the analysis is provided.

A. Signal processing

The initial phase of the data analysis involves the processing of the signals from the scintillators recorded by the digitizers. For each waveform, the total charge and the related timestamp are obtained. To enhance time resolution, a correction is applied to the timestamps using the constant fraction discrimination algorithm (CFD) [45–47]. The events recorded by the scintillators during the measurements are a mix of neutrons coming from elastic or inelastic scattering on the sample, and photons from the bremsstrahlung scattering on the sample, or from γ rays emitted via the inelastic scattering or neutron capture on the sample or the materials around the spectrometer. To discriminate between photon and neutron induced events the charge integration method was used. The signals were integrated over short and long time intervals, and the pulse shape discrimination (PSD) factor was defined as the ratio between the integral of the tail of the pulse to the total integrated charge [48–50]. In Fig. 4 an example of the time-of-flight distribution after applying the pulse shape discrimination for one of the detectors placed at the 100.6° detection angle is presented.

B. Detectors characterization

After the completion of signal processing, the subsequent stage involves characterizing the response function $R(L,E)$ of the detectors, which signifies the likelihood of a particle with energy E generating a light pulse with amplitude L. The methodology employed in this study combines measurements and Monte Carlo simulations as detailed in Refs. [51–54]. For every new experiment performed at the ELISA spectrometer, the detectors undergo a new complete characterization. This process is crucial for evaluating detector stability and detecting any issues that may have emerged during the measurements.

Starting with the parametrization of the resolution function, a set of calibration measurements using five γ-ray sources (^{137}Cs, ^{207}Bi, ^{22}Na, ^{232}Th, AmBe) were carried out

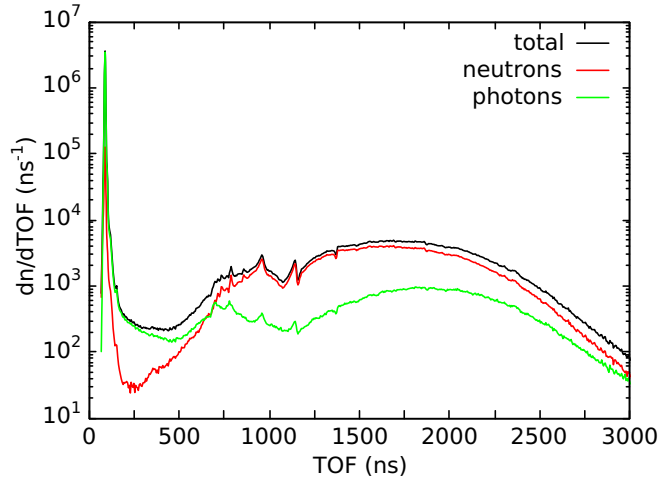

FIG. 4. Time-of-flight spectra from one of the detectors placed at the 100.6° detection angle during the thin sample measurement. The total number of recorded events (black line) along with the number of neutron (red line) and photon (green line) events individually, resulting from the pulse shape discrimination, are presented.

at the beginning and during the experiments to check the stability of the detectors. Additionally, Monte Carlo simulations of these measurements were performed using the MCNP6.2 code [55,56]. The simulated light output distributions were then fitted to the experimental data. In Fig. 5 an example of this procedure is presented for the case of the ^{207}Bi source for one of the EJ301 detectors. Through this fitting process, the final parameters for the resolution function specific to each detector were derived.

For the neutron response, experimental light output distributions for quasi-monoenergetic neutrons were obtained by selecting short time-of-flight intervals of 5 ns duration. Equivalent simulated distributions were calculated utilizing the MCNP6.2 code. Subsequently, the simulated neutron

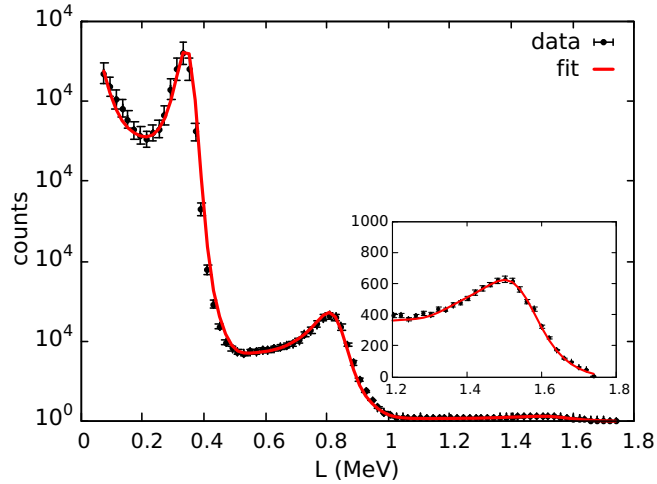

FIG. 5. Fit of the simulated resolution-folded response (red line) to the experimental data (black points) for the ^{207}Bi source, for an EJ301 detector. The three peaks correspond to the Compton edges of the three primary γ rays emitted by ^{207}Bi.

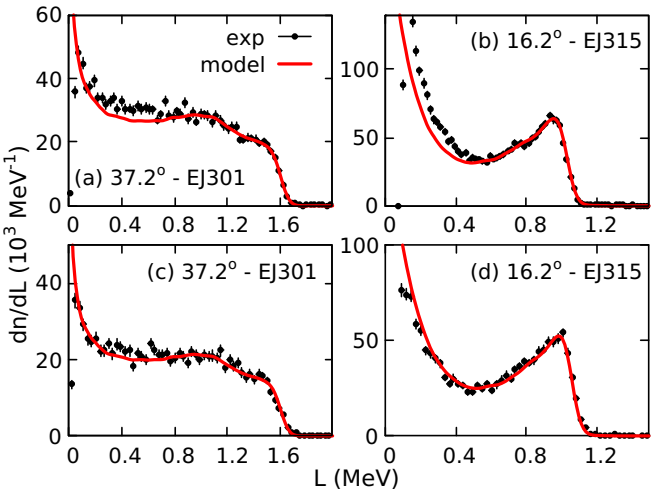

FIG. 6. Light output distributions from the thick [(a) and (b)] and thin [(c) and (d)] sample measurements. The graphs correspond to two different detection angles coming from the two different detector types (EJ301 and EJ315) for incident neutron energies $4.33 \leqslant E_n \leqslant 4.38$ MeV. The experimental data (black points) are presented along with their associated response models $R_{\rm fit}(L, E_{\rm el})$ (red line).

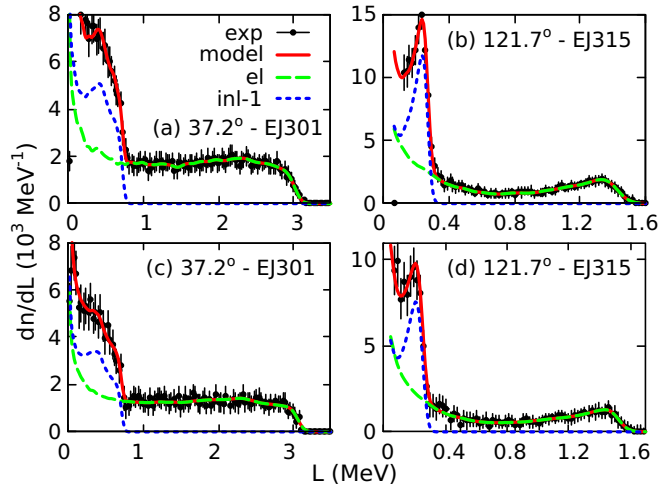

FIG. 7. Light output distributions for the incident neutron energies $6.95 \leqslant E_n \leqslant 7.05$ MeV from the thick [(a) and (b)] and thin [(c) and (d)] sample measurements. The experimental values (exp) are presented along with their associated response models (model) and their different components from elastic (el) and inelastic (inl-1) scattering from the first excited state of ^{12}C.

response was fitted to the experimental data and a set of parameters describing the light output function provided by Kornilov *et al.* [53] was extracted for every neutron energy. Ultimately, the diverse sets of parameters acquired from each energy interval were fine-tuned to derive a set of values optimized for the entire neutron energy range. In the case of the thick sample data two global models were developed, one for all the EJ301 and another one for all the EJ315 detectors, while for the thin sample data a different response function model was developed for each detector separately. In Fig. 6 an example of the resulting simulated detector response models for the thick and thin sample measurements are presented for a specific 5 ns interval, from 949 to 954 ns, that corresponds to neutron incident energies between 4.33 and 4.38 MeV.

C. Neutron elastic scattered events

Before extracting the number for neutron elastic scattering events, the background contribution needs to be taken into account. Events related to background are generated when beam neutrons interact one or more times in the air and surrounding materials before reaching the detectors. To address this contribution, measurements without the samples (sample-out) were conducted and then subtracted from the measurements with the samples in place (sample-in). The two different measurements were normalized based on the number of fission fragments recorded in the ionization chamber.

Once the neutron time-of-flight spectra have been extracted, following the removal of photons and background contribution, the separation between events coming from elastic and inelastic scattering took place. Since ^{12}C has the inelastic scattering threshold at 4.4398 MeV, neutrons with an incident energy above that threshold can be also scattered inelastically. To achieve a proper separation between detected neutrons originating from the different scattering processes, every light output distributions that corresponds to every 5 ns time-of-flight interval was carefully analyzed. In Fig. 7 examples of such light output distributions from both the thick and thin sample measurements are presented, for each type of detector, placed at two different detection angles. The chosen time-of-flight interval (750 to 755 ns) corresponds to incident neutrons with energies above the inelastic scattering threshold, specifically between 6.95 and 7.05 MeV. By performing kinematic calculations, the energies of the neutrons that were scattered elastically $E_{\rm el}$ or inelastically $E_{\rm inl}$ for every time-of-flight interval was determined. The two different neutron energies generate a different light output distribution that overlap in each 5 ns time-of-flight interval as seen in Fig. 7. The contribution from inelastic scattering induced events was excluded by applying a proper threshold. The threshold is placed at the maximum light output produced by an inelastic event taking into account the resolution broadening of the detector. The number of elastic scattering events is then extracted using the formula

$$\langle N_{\rm el}\rangle_{\Delta t}(\theta) = \frac{1}{\epsilon(E_{\rm el})|_{L_{\rm thr}}\Delta\Omega}\int_{L_{\rm thr}} R_{\rm fit}(L, E_{\rm el})dL, \qquad (3)$$

where $\langle N_{\rm el}\rangle_{\Delta t}$ is the number of elastic scattering events per $\Delta t = 5$ ns time-of-flight interval and detection angle, $\Delta\Omega$ is the detector opening angle, and $\epsilon(E_{\rm el})|_{L_{\rm thr}}$ is the intrinsic efficiency of each detector with respect to the detected neutron energy $E_{\rm el}$ calculated for the threshold value $L_{\rm thr}$ using $\epsilon(E_{\rm el})|_{L_{\rm thr}} = \int_{L_{\rm thr}} R(L, E_{\rm el})dL$.

D. Multiple scattering correction

The extracted number of neutron elastic scattering events needs to be corrected for multiple scattering, i.e., beam neutrons that scattered twice or more in the carbon samples and then got detected by one of the scintillators. In the current study, the correction factor ($f_{\rm msc}$) was determined through

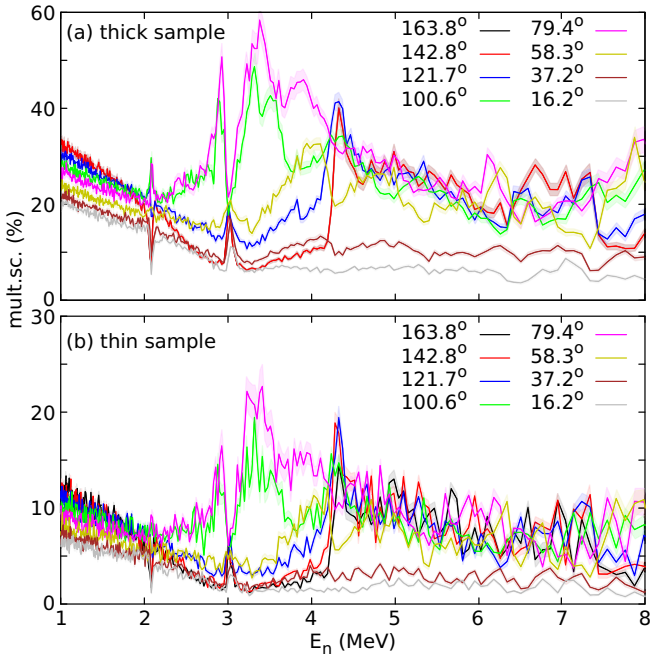

FIG. 8. Percentage of the multiple scattering correction as a function of the incident neutron energy, for both the thick (a) and the thin (b) sample measurements, at the eight different detection angles.

Monte Carlo simulations using the MCNP6.2 code. The simulation input included a complete description of the geometry of the spectrometer and the neutron source, based on the actual beam properties during the measurement of the samples. The MCNP-PTRAC option was exploited, to get an output with a complete history of the neutrons that reached the detectors. The correction factor was then determined as the ratio of detected neutron events that interacted more than once with the sample to the total number of detected events. This approach offers a time-of-flight dependent correction for each detection angle, and is applied to the differential scattering yield via the formula $N'_{\rm el} = (1 - f_{\rm msc})N_{\rm el}$. In Fig. 8 the resulting multiple scattering correction is presented. It is observed that in the case of the thick sample the correction is almost double compared to the thin one, over the whole neutron energy range and for all detection angles, and becomes significant for angles close to 90°, reaching a correction value of almost 60%.

E. Uncertainties

The total uncertainty of the final results was calculated using the law of error propagation, accounting for all individual contributions. In Table III the different systematic uncertainties that contributed in the data analysis are presented. In the present work, the statistical uncertainty in the cross section arises from the number of neutron elastic scattered events from the $^{\rm nat}$C samples that got detected, and the fission fragment yield of the ^{235}U deposits in the ionization chamber.

IV. RESULTS

The resulting angular distributions of neutron elastic scattering on natural carbon, with respect to the incident neutron energy, for the eight different detection angles, are presented in Fig. 9. The results, both for the thick and thin sample measurements, are compared with the JEFF-3.3, ENDF/B-VIII.0, and JENDL-5 evaluations, folded with the experimental energy resolution. There is a relatively good agreement between experimental and evaluated values over the whole neutron energy range, especially for the thin sample measurements. Between the two different measurements, discrepancies are observed for energies below 2 MeV incident energy in some detection angles. Specifically in the backward angles [Figs. 9(a)–9(c)], in the energy region from 1 to 1.2 MeV, the results coming from the thick sample data are overestimated, the main reason for that is the fact that the two global models developed to describe the neutron response for all the EJ301 and EJ315 detectors in the case of the thick sample are proven to perform poorly for low light output distributions, i.e., neutron energies below 2 MeV [39]. Additionally, big discrepancies between the two measurements are observed in almost the whole neutron energy range for the 100.6° and 79.4° detection angles. This is due to the high multiple scattering correction for the thick sample data for the detection angles close to 90° (see Fig. 8). Out of the three evaluations included in the figure, ENDF/B-VIII.0 seems to perform better compared to the data of this work in all detection angles, while in the cases of JEFF-3.3 and JENDL-5 discrepancies are observed especially for the 100.6° detection angle. The total uncertainties on the angular distributions vary from 3% to 10% for the thick sample, and from 3% to 14% for the thin sample.

In Fig. 10, the differential elastic scattering neutron cross sections are given for a selection of neutron energies as a function of the detection angle θ, along with the available data in the EXFOR library and the cross section values provided by the JEFF-3.3, ENDF/B-VIII.0, and JENDL-5 evaluations. Eight 5 ns time of flight intervals have been selected for this comparison, that cover most of the neutron incident energies that have been reported from other experiments in the literature (see Table I). There is a good agreement between the results of this work and the experimental values available in the EXFOR library. The results are in agreement within uncertainty with the most recent data reported by Ramirez *et al.* (2022) [38] using quasi-monoenergetic neutron beams. Significant discrepancies between experimental data and evaluations are observed only in Fig. 10(c), for the interval that corresponds to 3 MeV incident neutron energy, where the evaluations are following a somewhat different trend compared to the majority of the experimental data. This is due

TABLE III. Systematic relative uncertainties involved in the carbon data analysis.

Contribution	Thick	Thin
Sample areal density	0.2%	0.3%
Multiple scattering correction	5–9%	3–8%
Fission chamber efficiency	1%	
^{235}U(n, f) cross section	1.1–1.2%	
^{235}U deposits mass	0.001%	

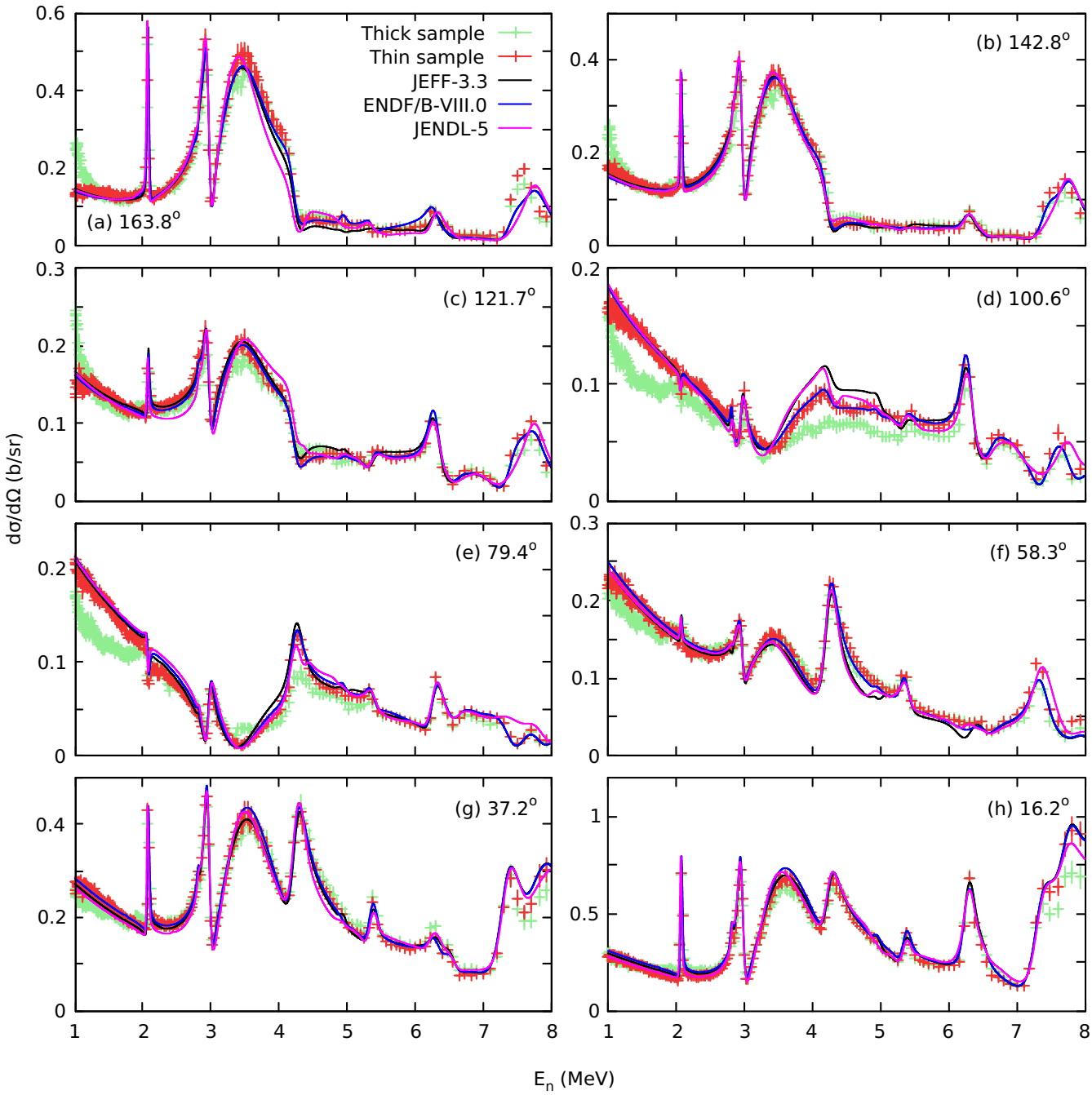

FIG. 9. Differential cross sections of neutron elastic scattering on ^{nat}C as a function of the incident neutron energy at the eight detection angles. The experimental cross sections are compared with the evaluated values provided by the JEFF-3.3 [5], ENDF/B-VIII.0 [8], and JENDL-5 [11] libraries folded with the experimental energy resolution.

to the quick change in the shape of the differential cross section in both backward and forward angles in this energy region. The cross section is falling rapidly from 2.9 to 3 MeV, where it reaches the minimum value, and then increases fast from 3 to 3.5 MeV. The resolution of the current measurements is not good enough to properly describe this dip in the cross section. In Fig. 11 the proposed cross sections of the ENDF/B-VIII.0 evaluation for the lowest (2.981 MeV) and the highest (3.007 MeV) neutron energies of the 5 ns time of flight interval chosen to describe the cross section at 3 MeV are presented along with the experimental results. The strong fluctuating behavior of the cross section is observed. As expected, due to the limitations of the resolution of the measurement, the experimental results are lying in the middle of the proposed values by ENDF/B-VIII.0.

The results of the angle-integrated neutron elastic scattering cross sections are presented in Fig. 12. The data are compared to the available cross sections data in the EXFOR library and the evaluated values provided by the JEFF-3.3, ENDF/B-VIII.0, and JENDL-5 libraries folded with the

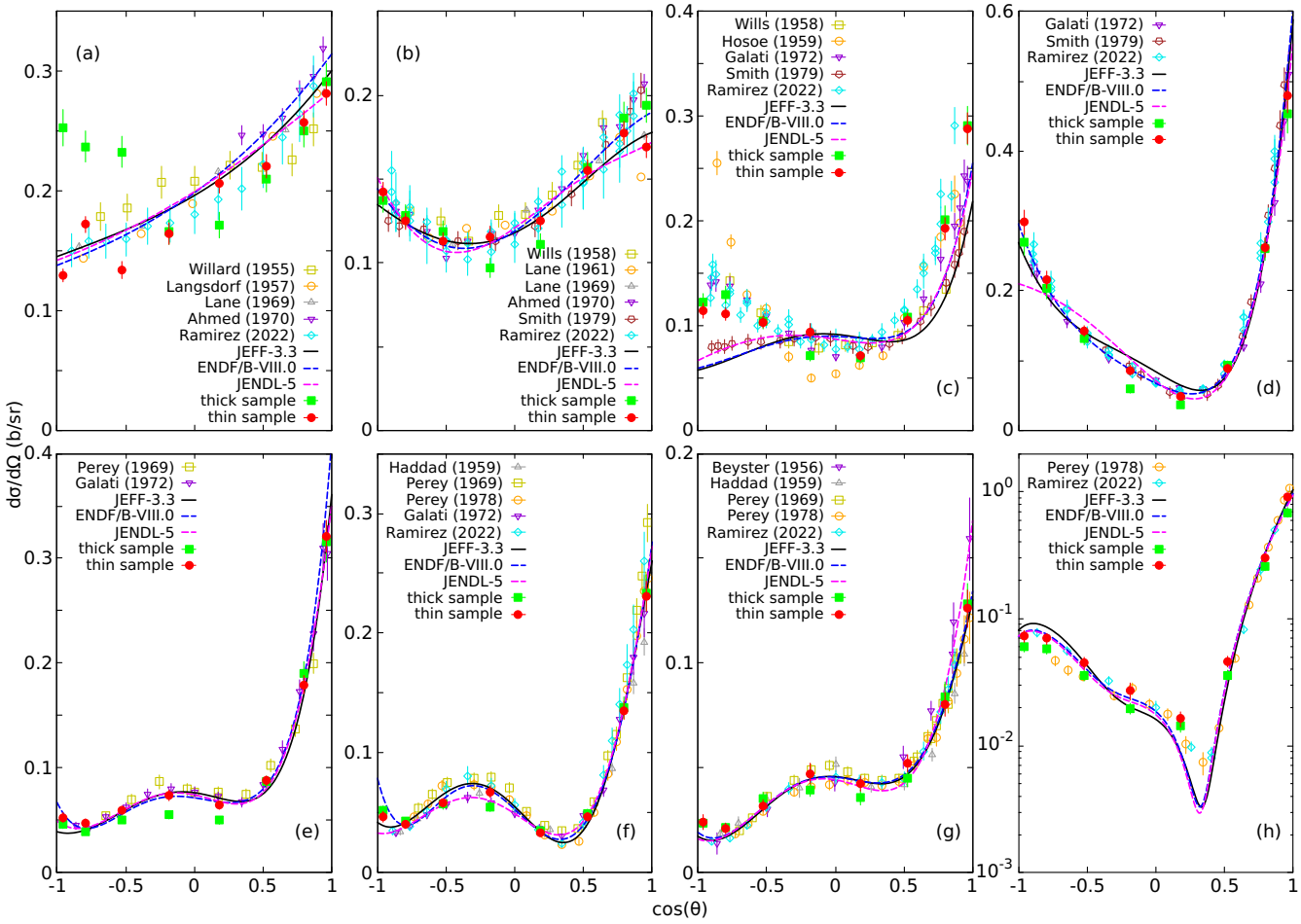

FIG. 10. Comparison of differential cross sections of neutron elastic scattering on ^{nat}C as a function of the cosine of the scattering angle θ, with data available in the EXFOR library [13] and the angular distributions provided in the JEFF-3.3 [5], ENDF/B-VIII.0 [8], and JENDL-5 [11] evaluations. Eight 5 ns time of flight intervals have been selected, that correspond to the following neutron energy ranges: (a) $E = 0.998$–1.003 MeV, (b) $E = 1.994$–2.009 MeV, (c) $E = 2.981$–3.007 MeV, (d) $E = 3.987$–4.028 MeV, (e) $E = 4.990$–5.047 MeV, (f) $E = 5.956$–6.033 MeV, (g) $E = 6.953$–7.047 MeV, (h) $E = 7.872$–7.986 MeV.

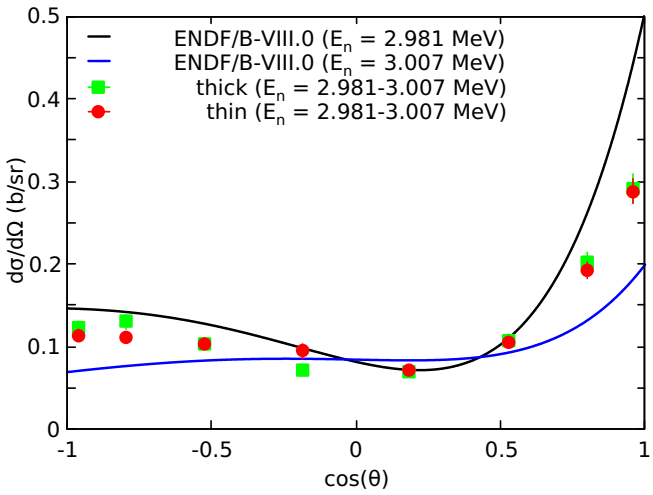

FIG. 11. Comparison of the differential cross sections for the 5 ns interval that corresponds to the neutron energy range $E_n = 2.981$–3.007 MeV.

experimental energy resolution. The results of this work are in good agreement, within uncertainties, with the other experimental values and the evaluation libraries. The effect of the discrepancies on the angular distributions reported earlier between thick and thin sample for energies below 2 MeV is also observed here, because in the case of the thick sample data the resulting angle-integrated cross section is underestimated. The total uncertainties on the angle-integrated cross sections varied from 5% to 10% for the thick sample, and from 3% to 8% for the thin sample.

V. CONCLUSIONS

In this study, new measurements of the double differential cross section of neutron elastic scattering on natural carbon were carried out at the GELINA time-of-flight facility. The ELISA spectrometer was employed, a setup consisting of 32 liquid organic scintillators for the detection of the scattered neutrons, and a ^{235}U ionization chamber for the measurement of the neutron flux. Two natural carbon samples with different

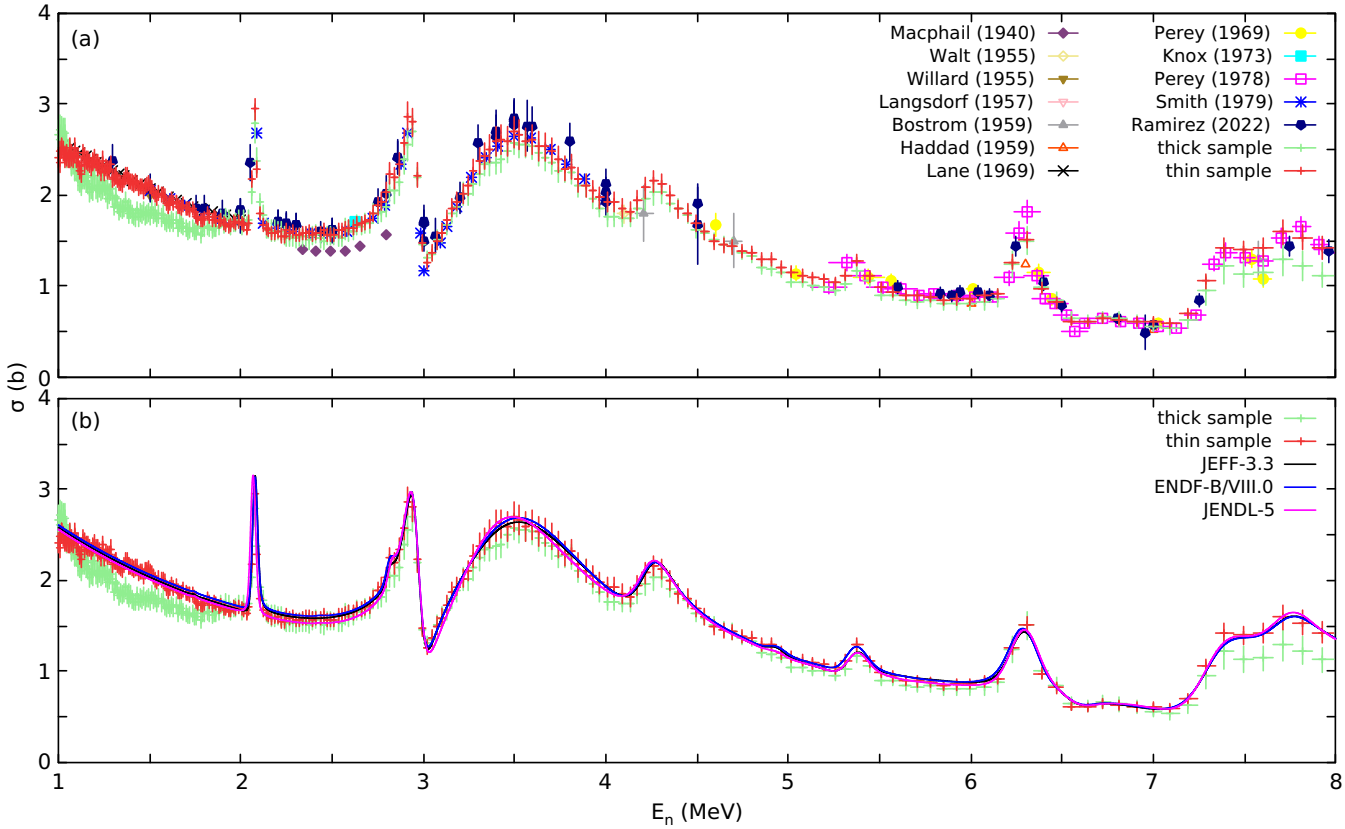

FIG. 12. Angle-integrated cross section of neutron elastic scattering on ^{nat}C as a function of the incident neutron energy compared with (a) the data available in the EXFOR library [13], and (b) the JEFF-3.3 [5], ENDF/B-VIII.0 [8], and JENDL-5 [11] libraries folded with the experimental energy resolution.

thicknesses were used in order to study the effect of the multiple scattering in the final results. The data analysis is shortly described. The process includes the modeling of the response functions of the detectors by combining measurements and Monte Carlo simulations, special treatment of the recorded signals, the subtraction of the background contribution based on the sample-out/sample-in measurements, the extraction of the neutron scattered yield, and the correction for multiple scattering via Monte Carlo simulations. Two different methodologies were studied related to the development of the response functions of the scintillators, one where a global model was developed for each type of detector (two models in total), and an other one based on a per-detector model (32 models in total). This work illustrates the better performance of the per-detector models for low neutron energies, i.e., low light output distributions. The differential cross section was calculated at 8 detection angles using Eq. (2) and the integral cross section using the Gauss-Legendre quadrature rule Eq. (1). Discrepancies in the angular distributions between thick and thin sample data are observed, especially in angles close to 90° where the multiple scattering correction is becoming significant in the case of the thick sample. This indicates the need for using thin samples during these kind of measurements. The final results were compared to the data available in the EXFOR library and the JEFF-3.3, ENDF-B/VIII.0, and JENDL-5 evaluations.

These were the first experimental measurements providing high-resolution data for neutron elastic scattering on natural carbon in the energy range of 1 to 8 MeV. The total uncertainties vary from 3% to 14% for the differential cross sections, and from 3% to 10% for the angle integrated cross section. The results of the thin sample are in overall good agreement with the other experimental data available in the EXFOR library and the most recent nuclear data evaluations, with ENDF/B-VIII.0 having the best agreement. The new values, mainly the thin sample data, can be used in future evaluations and assist in the extension of the standard cross section to energies above 1.8 MeV.

ACKNOWLEDGMENTS

The authors would like to thank the GELINA staff for providing the conditions needed for this experiment. This work was partially supported by the Commissariat á l'énergie atomique et aux énergies alternatives (CEA) through the SINET project, and by the European Commission through the EUFRAT [57], and ARIEL (EURATOM research and training program 2014-2018 under Grant Agreement No. 847594) [58] projects.

[1] K. Dasgupta, M. Roy, A. Tyagi, S. Kulshreshtha, R. Venugopalan, and D. Sathiyamoorthy, Novel isotropic high-density amorphous carbon composites for moderator applications in low-temperature thermal reactors, Compos. Sci. Technol. **67**, 1794 (2007).

[2] R. Venugopalan, V. Alur, A. Patra, R. Acharya, and D. Srivastava, Investigations on neutron irradiated 3D carbon fibre reinforced carbon composite material, J. Nucl. Mater. **502**, 276 (2018).

[3] X.-W. Zhou, Y. Yang, J. Song, Z. ming Lu, J. Zhang, B. Liu, and Y. ping Tang, Carbon materials in a high temperature gas-cooled reactor pebble-bed module, New Carbon Mater. **33**, 97 (2018).

[4] A. Carlson, V. Pronyaev, R. Capote, G. Hale, Z.-P. Chen, I. Duran, F.-J. Hambsch, S. Kunieda, W. Mannhart, B. Marcinkevicius, R. Nelson, D. Neudecker, G. Noguere, M. Paris, S. Simakov, P. Schillebeeckx, D. Smith, X. Tao, A. Trkov, A. Wallner *et al.*, Evaluation of the neutron data standards, Nucl. Data Sheets **148**, 143 (2018).

[5] A. Plompen, O. Cabellos, C. De Saint Jean, M. Fleming, A. Algora, M. Angelone, P. Archier, E. Bauge, O. Bersillon, A. Blokhin, F. Cantargi, A. Chebboubi, C. J. Diez, H. Duarte, E. Dupont, J. Dyrda, B. Erasmus, L. Fiorito, U. Fischer, D. Flammini *et al.*, The joint evaluated fission and fusion nuclear data library, JEFF-3.3, Eur. Phys. J. A **56**, 181 (2020).

[6] C. Y. Fu, Evaluated cross sections for neutron scattering from natural carbon below 2 MeV including R matrix fits to ^{13}C resonances, Nucl. Sci. Eng. **106**, 494 (1990).

[7] C. Y. Fu and F. G. Perey, Neutron scattering cross sections of carbon below 2 MeV recommended from R-matrix fits to data, At. Data Nucl. Data Tables **22**, 249 (1978).

[8] D. Brown, M. Chadwick, R. Capote, A. Kahler, A. Trkov, M. Herman, A. Sonzogni, Y. Danon, A. Carlson, M. Dunn, D. Smith, G. Hale, G. Arbanas, R. Arcilla, C. Bates, B. Beck, B. Becker, F. Brown, R. Casperson, J. Conlin *et al.*, ENDF/B-VIII.0: The 8th major release of the nuclear reaction data library with CIELO-project cross sections, new standards and thermal scattering data, Nucl. Data Sheets **148**, 1 (2018).

[9] D. C. Dodder, G. M. Hale, and K. Witte, The energy dependent analysis code, Los Alamos National Laboratory (unpublished).

[10] G. Hale and P. Young, n + ^{12}C cross sections from an R-matrix analysis of reactions in the ^{13}C system, Nucl. Data Sheets **118**, 165 (2014).

[11] O. Iwamoto, N. Iwamoto, S. Kunieda, F. Minato, S. Nakayama, Y. Abe, K. Tsubakihara, S. Okumura, C. Ishizuka, T. Yoshida, S. Chiba, N. Otuka, J.-C. Sublet, H. Iwamoto, K. Yamamoto, Y. Nagaya, K. Tada, C. Konno, N. Matsuda, K. Yokoyama *et al.*, Japanese evaluated nuclear data library version 5: JENDL-5, J. Nucl. Sci. Technol. **60**, 1 (2023).

[12] S. Kunieda, Present status of an R-matrix analysis code AMUR for cross-section evaluation in resolved resonance region, EPJ Web Conf. **284**, 03014 (2023).

[13] N. Otuka, E. Dupont, V. Semkova, B. Pritychenko, A. I. Blokhin, M. Aikawa, S. Babykina, M. Bossant, G. Chen, S. Dunaeva, R. A. Forrest, T. Fukahori, N. Furutachi, S. Ganesan, Z. Ge, O. O. Gritzay, M. Herman, S. Hlavač, K. Katō, B. Lalremruata *et al.*, Towards a more complete and accurate experimental nuclear reaction data library (EXFOR): International collaboration between nuclear reaction data centres (NRDC), Nucl. Data Sheets **120**, 272 (2014).

[14] M. R. MacPhail, Anomalous scattering of fast neutrons, Phys. Rev. **57**, 669 (1940).

[15] R. N. Little, B. P. Leonard, J. T. Prud'homme, and L. D. Vincent, Liquid scintillator measurements of angular elastic scattering of neutrons from carbon, aluminum, and sulfur, Phys. Rev. **98**, 634 (1955).

[16] B. Jennings, J. Weddell, I. Alexeff, and R. L. Hellens, Scattering of 4.4-MeV neutrons by iron and carbon, Phys. Rev. **98**, 582 (1955).

[17] M. Walt and J. R. Beyster, Interaction of 4.1-MeV neutrons with nuclei, Phys. Rev. **98**, 677 (1955).

[18] H. B. Willard, J. K. Bair, and J. D. Kington, Elastic scattering angular distributions of fast neutrons on light nuclei, Phys. Rev. **98**, 669 (1955).

[19] C. O. Muehlhause, S. D. Bloom, H. E. Wegner, and G. N. Glasoe, Neutron scattering from iron and carbon by time-of-flight, Phys. Rev. **103**, 720 (1956).

[20] J. R. Beyster, M. Walt, and E. W. Salmi, Interaction of 1.0-, 1.77-, 2.5-, 3.25-, and 7.0-MeV neutrons with nuclei, Phys. Rev. **104**, 1319 (1956).

[21] A. Langsdorf, R. O. Lane, and J. E. Monahan, Angular distributions of scattered neutrons, Phys. Rev. **107**, 1077 (1957).

[22] J. E. Wills, J. K. Bair, H. O. Cohn, and H. B. Willard, Scattering of fast neutrons from C^{12} and F^{19}, Phys. Rev. **109**, 891 (1958).

[23] M. Hosoe and S. Suzuki, Gamma rays from neutron inelastic scattering of magnesium, aluminum, iron and bismuth, J. Phys. Soc. Jpn. **14**, 699 (1959).

[24] E. Haddad and D. D. Phillips, Elastic and inelastic scattering of neutrons from C^{12}, Bull. Am. Phys. Soc. **4**, 358 (1959).

[25] N. A. Bostrom, I. L. Morgan, J. T. Prud'homme, P. L. Okhuysen, and O. M. Hudson, Jr., Neutron interactions in Lithium, Carbon, Nitrogen, Aluminum, Argon, Manganese, Yttrium, Zirconium, Radiolead and Bismuth, Wright Air Development Center Report No. WADC-TN-59-10710, 1959 (unpublished).

[26] R.O Lane, A. Langsdorf, J. Monahan, and A. Elwyn, The angular distributions of neutrons scattered from various nuclei, Ann. Phys. **12**, 135 (1961).

[27] R. O. Lane, R. D. Koshel, and J. E. Monahan, Polarization and differential cross section for neutrons scattered from ^{12}C, Phys. Rev. **188**, 1618 (1969).

[28] F. G. Perey and W. E. Kinney, Carbon neutron elastic-and inelastic-scattering cross sections from 4.5 to 8.5 MeV, Oak Ridge National Laboratory, Report No. 4441 (1969).

[29] N. Ahmed, M. Coppola, and H. H. Knitter, Measurements of neutron elastic scattering from carbon in the energy region of 0.50 to 2.00 MeV, Nuclear Data Reactors Conf. **1**, 177 (1970).

[30] F. D. McDaniel, M. W. McDonald, M. F. Steuer, and R. M. Wood, Spin-flip probability in the inelastic scattering of 7.48-MeV neutrons from the 4.43-MeV state of ^{12}C, Phys. Rev. C **6**, 1181 (1972).

[31] W. Galati, J. D. Brandenberger, and J. L. Weil, Scattering of neutrons by carbon from 3 to 7 MeV, Phys. Rev. C **5**, 1508 (1972).

[32] H. Knox, J. Cox, R. Finlay, and R. Lane, Differential cross section and polarization for 2.63 MeV neutrons scattered from ^{12}C, Nucl. Phys. A **217**, 611 (1973).

[33] D. E. Velkley, J. D. Brandenberger, D. W. Glasgow, M. T. McEllistrem, J. C. Manthuruthil, and C. P. Poirier, Scattering

of neutrons by carbon from 7 to 9 MeV, Phys. Rev. C **7**, 1736 (1973).

[34] C. E. Hollandsworth, W. P. Bucher, J. Youngblood, and A. Niiler, Cross sections for forward-angle elastic scattering of 7.55 MeV neutrons- A survey, Ballistic Research Labs, Report No. 1764 (1975).

[35] F. G. Perey and W. E. Kinney, Elastic and inelastic scattering cross sections in the energy range 5.2-8.7 MeV, U.S. AEC Nuclear Cross Sections Advisory Committee, Report No. 42, 190 (1978).

[36] A. Smith, R. Holt, and J. Whalen, Neutron interaction with carbon-12 in the few-MeV region, Nucl. Sci. Eng. **70**, 281 (1979).

[37] E. Pirovano, R. Beyer, M. Dietz, A. R. Junghans, S. E. Müller, R. Nolte, M. Nyman, A. J. M. Plompen, M. Röder, T. Szücs, and M. P. Takacs, Cross section and neutron angular distribution measurements of neutron scattering on natural iron, Phys. Rev. C **99**, 024601 (2019).

[38] A. Ramirez, E. Peters, J. Vanhoy, S. Hicks, L. Alasagas, D. Alcorn-Dominguez, S. Block, S. Byrd, E. Chouinard, B. Combs, B. Crider, E. Derdyn, L. Downes, J. Erlanson, S. Evans, A. French, E. Garza, J. Girgis, T. Harrison, S. Henderson *et al.*, Neutron elastic and inelastic scattering differential cross sections on carbon, Nucl. Phys. A **1023**, 122446 (2022).

[39] E. Pirovano, Neutron scattering cross section measurements with a new scintillator array, Ph.D. thesis, Ghent University, 2017.

[40] W. Mondelaers and P. Schillebeeckx, Notiziaro Neutroni e Luce di Sincrotrone **11**, 19 (2006).

[41] D. Ene, C. Borcea, S. Kopecky, W. Mondelaers, A. Negret, and A. Plompen, Global characterisation of the GELINA facility for high-resolution neutron time-of-flight measurements by Monte Carlo simulations, Nucl. Instrum. Methods Phys. Res. A **618**, 54 (2010).

[42] E. Pirovano, R. Beyer, A. Junghans, R. Nolte, M. Nyman, and A. Plompen, Measurements of neutron scattering angular distributions with a new scintillator setup, EPJ Web Conf. **146**, 11008 (2017).

[43] M. Nyman, T. Adam, C. Borcea, M. Boromiza, P. Dessagne, G. Henning, M. Kerveno, A. Negret, A. Olacel, E. Pirovano *et al.*, New equipment for neutron scattering cross-section measurements at GELINA, EPJ Web Conf. **239**, 17003 (2020).

[44] G. Gkatis, M. Diakaki, G. Noguere, M. Nyman, A. Oprea, C. Paradela, E. Pirovano, and A. J. M. Plompen, Cross section measurements of neutron elastic and inelastic scattering on ^{54}Fe, Phys. Rev. C **109**, 034612 (2024).

[45] D. Gedcke and W. McDonald, A constant fraction of pulse height trigger for optimum time resolution, Nucl. Instrum. Methods **55**, 377 (1967).

[46] L. Bardelli, G. Poggi, M. Bini, G. Pasquali, and N. Taccetti, Time measurements by means of digital sampling techniques: A study case of 100ps FWHM time resolution with a 100MSample/s, 12bit digitizer, Nucl. Instrum. Methods Phys. Res. A **521**, 480 (2004).

[47] M. A. Nelson, B. D. Rooney, D. R. Dinwiddie, and G. S. Brunson, Analysis of digital timing methods with BaF_2 scintillators, Nucl. Instrum. Methods Phys. Res. A **505**, 324 (2003).

[48] I. A. Pawełczak, S. Ouedraogo, A. Glenn, R. Wurtz, and L. Nakae, Studies of neutron-γ pulse shape discrimination in EJ-309 liquid scintillator using charge integration method, Nucl. Instrum. Methods Phys. Res. A **711**, 21 (2013).

[49] F. Brooks, A scintillation counter with neutron and gamma-ray discriminators, Nucl. Instrum. Methods **4**, 151 (1959).

[50] J. Polack, M. Flaska, A. Enqvist, C. Sosa, C. Lawrence, and S. Pozzi, An algorithm for charge-integration, pulse-shape discrimination and estimation of neutron/photon misclassification in organic scintillators, Nucl. Instrum. Methods Phys. Res. A **795**, 253 (2015).

[51] A. Tomanin, J. Paepen, P. Schillebeeckx, R. Wynants, R. Nolte, and A. Lavietes, Characterization of a cubic EJ-309 liquid scintillator detector, Nucl. Instrum. Methods Phys. Res. A **756**, 45 (2014).

[52] H. Klein and S. Neumann, Neutron and photon spectrometry with liquid scintillation detectors in mixed fields, Nucl. Instrum. Methods Phys. Res. A **476**, 132 (2002).

[53] N. Kornilov, I. Fabry, S. Oberstedt, and F.-J. Hambsch, Total characterization of neutron detectors with a ^{252}Cf source and a new light output determination, Nucl. Instrum. Methods Phys. Res. A **599**, 226 (2009).

[54] H. Klein, Neutron spectrometry in mixed fields: NE213/BC501A liquid scintillation spectrometers, Radiat. Prot. Dosim. **107**, 95 (2003).

[55] C. J. Werner, J. Bull, C. Solomon, F. Brown, G. McKinney, M. Rising, D. Dixon, R. Martz, H. Hughes, L. Cox *et al.*, MCNP6.2 release notes, Los Alamos National Laboratory, Report No. LA-UR-18-20808 (2018).

[56] C. J. Werner, J. C. Armstrong, F. B. Brown, J. S. Bull, L. Casswell, L. J. Cox, D. A. Dixon, R. A. Forster III, J. T. Goorley, H. G. Hughes III *et al.*, MCNP user's manual-code version 6.2, Los Alamos National Laboratory, Report No. LA-UR-17-29981 (2017), http://permalink.lanl.gov/object/tr?what=info:lanl-repo/lareport/LA-UR-17-29981.

[57] S. Oberstedt, G. Sibbens, S. Kopecky, M. Nyman, Y. Aregbe, A. Göök, A. Plompen, C. Paradela, M. Hult, J. Heyse, and P. Schillebeeckx, EUFRAT, Open access to the nuclear research infrastructure at JRC Geel – Summary report 2017-2018 (European Commission, Joint Research Centre, Publications Office, 2018), https://data.europa.eu/doi/10.2760/798329.

[58] C. Franzen, A. Junghans, E. M. Gonzalez, and A. J. M. Plompen, ARIEL & SANDA nuclear data activities, EPJ Nucl. Sci. Technol. **8**, 19 (2022).